催化学报
2012 Chinese Journal of Catalysis Vol. 33 No. 9

文章编号: 0253-9837(2012)09-1480-06 国际版 DOI: 10.1016/S1872-2067(11)60415-4 研究论文: 1480–1485

介孔 TiO_2 晶须担载 Au 的热稳定性

马璇璇[1], 朱银华[2], 李力成[1], 王昌松[1], 陆小华[1], 杨祝红[1,*]

[1]南京工业大学材料化学工程国家重点实验室, 江苏南京 210009

[2]江苏华兰药用新材料股份有限公司技术研究中心, 江苏无锡 214443

摘要: 以二钛酸钾晶须为前驱体, 通过固相烧结工艺制备了介孔 TiO_2 晶须, 然后使用沉积沉淀法将 Au 纳米颗粒担载于其上, 并采用低温 N_2 吸附-脱附、X 射线衍射及透射电镜等技术对催化剂的形貌和结构进行了表征, 以 $NaBH_4$ 还原对硝基苯酚 (PNP) 为探针反应, 评价了催化剂的活性及稳定性. 结果表明, 500 °C 热处理前后, 介孔 TiO_2 负载的 Au 纳米颗粒的平均粒径变化不大, 且催化 PNP 还原活性得到了很好的保持. 这主要与介孔 TiO_2 晶须独特的双晶构型及介孔结构有关.

关键词: 纳米金; 热稳定性; 介孔氧化钛; 双晶; 对硝基苯酚; 还原

中图分类号: O643 **文献标识码**: A

收稿日期: 2012-03-30. 接受日期: 2012-05-26.

*通讯联系人. 电话/传真: (025)83588063; 电子信箱: zhhyang@njut.edu.cn

基金来源: 国家自然科学基金 (20736002, 20976080, 21136001); 国家高技术研究发展计划 (863 计划, 2006AA03Z455).

本文的英文电子版(国际版)由Elsevier出版社在ScienceDirect上出版(http://www.sciencedirect.com/science/journal/18722067).

Thermal Stability of Gold Catalyst Supported on Mesoporous Titania Nanofibers

MA Xuanxuan[1], ZHU Yinhua[2], LI Licheng[1], WANG Changsong[1], LU Xiaohua[1], YANG Zhuhong[1,*]

[1]*State Key Laboratory of Materials-oriented Chemical Engineering, Nanjing University of Technology, Nanjing 210009, Jiangsu, China*

[2]*Technology Research Institute, Jiangsu Hualan New Pharmaceutical Material Co. Ltd., Wuxi 214443, Jiangsu, China*

Abstract: By deposition-precipitation with urea method, gold was loaded on mesoporous TiO_2 whisker, which was prepared from a potassium titanate whisker precursor through solid phase sintering process. The morphology and structure of these as-prepared catalysts were characterized by N_2 adsorption-desorption, X-ray diffraction, and transmission electron microscopy. The reduction of 4-nitrophenol to 4-aminophenol by $NaBH_4$ was evaluated as a probe reaction. After calcination at high temperature, the activity of the catalysts supported on mesoporous TiO_2 nanofiber was well maintained, and the particle size of gold nanoparticles was hardly changed. This might be attributed to the peculiar crystallographic structure and mesoporous nanoarchitecture of the mesoporous TiO_2 whisker.

Key words: nanogold; thermal stability; mesoporous titania; bicrystal; *p*-nitrophenol; reduction

Received 30 March 2012. Accepted 26 May 2012.

**Corresponding author. Tel/Fax: +86-25-83588063; E-mail: zhhyang@njut.edu.cn*

This work was supported by the National Natural Science Foundation of China (20736002, 20976080, 21136001) and the National High Technology Research and Development Program of China (863 Program, 2006AA03Z455).

English edition available online at Elsevier ScienceDirect (http://www.sciencedirect.com/science/journal/18722067).

Supported nanogold catalysts have attracted much attention for their high activity and efficiency in various heterogeneous catalytic reactions [1–4]. Although the nature of the active sites is still debatable, it is widely accepted that well dispersed gold particles with high thermal stability and strong adhesive force are essential for developing advanced gold catalysts with stable performances [5,6]. High thermal stability assures less agglomeration of gold nanoparticles. Strong adhesion prevents the active components loss during the reaction processes. There are mainly two types of methods developed to improve the thermal stability of gold nanoparticles and their adhesion to support materials. One is

developing a support with proper nanostructures [7–9]. The other is modifying gold catalysts with oxide surface layers [10,11]. Due to the complexity and high cost of the synthetic process of the latter method, choosing porous substrates is considered as a more feasible way. Based on this concept, nanogold catalysts with high thermal stability and stable anchoring properties have been successively developed by confining the presynthesized gold clusters into hierarchic porous oxide materials [5,7,12].

Because of the high reactivity and possible strong metal support interaction (SMSI) effects [13], titania is thought to be the most prominent oxide support material for gold nanoparticles. However, the porous architectures of titania materials with high surface area always tend to collapse at high temperature, which further decrease the usability as a gold catalyst support. Besides, the complex synthetic procedures and residual impurities of porous titania architectures also limit their applications.

In our previous work, we synthesized a highly crystallized mesoporous titania nanofiber with high thermal stability, in which the specific surface area of 139 m^2/g was maintained after calcination at 500 °C for 2 h [14]. Our recent study also revealed that the mesoporous titania nanofiber prepared from $K_2Ti_2O_5$ was a core-shell structured TiO_2(B)-anatase bicrystalline titania (denoted as mb-TiO_2) [15,16]. Stable anchoring of Pt nanoparticles onto this core-shell structured titania resulted in a rather higher and more stable photocatalytic hydrogen production performance [17]. The mesoporous titania nanofiber was also used as a gold catalyst support [9,18]. Compared with commercial nonporous P25 (Degussa AG) gold loaded on mesoporous titania nanofiber performed a better activity in low-temperature CO oxidation. However, the thermal stability of the Au/TiO_2 catalyst based on the mesoporous bicrystalline titania was not evaluated yet. In the present paper, the Au/TiO_2 catalyst prepared by homogeneous deposition-precipitation method was treated at high temperature under inert atmosphere and then tested in the catalytic reduction of *p*-nitrophenol (PNP) to investigate its thermal stability.

1 Experimental

1.1 Preparation of TiO_2(B) coated mesoporous anatase nanofiber and gold catalysts

TiO_2(B) coated anatase nanofiber was prepared by following our previous work [15]. Calcination of the dried sample was performed in a muffle oven at 600 °C in air for 2 h. After cooling naturally, TiO_2(B) coated mesoporous anatase nanofibers were synthesized (denoted as mb-TiO_2).

Gold (2.0 wt%) was deposited on as-synthesized TiO_2 nanofibers by deposition-precipitation with urea method. In a typical procedure, excess urea (7.56 g) was dissolved in 300 ml of 0.52 mmol/L $HAuCl_4$ solution at room temperature. About 1.5 g titania support was then added into the yellow solution, the resulting mixture was heated at 80 °C for 3 h under vigorous stirring. The suspension was then filtered and washed several times until no chloride ions were detected by $AgNO_3$ solution. The solid product was oven-dried at 60 °C for 12 h and calcined at 300 °C for 2 h in static air before subsequent modification or activity evaluation.

In order to investigate the thermal stability of the nanogold catalyst, the fresh Au/mb-TiO_2 was further calcined at 500 °C for 2 h in flowing helium gas (50 ml/min) before activity test. The recalcined gold catalyst was denoted as Au/mb-TiO_2-R. For comparison, gold was loaded on commercial titania (P25, AEROXIDE) and recalcined following the same procedure. The recalcined Au/P25 was further denoted as Au/P25-R.

1.2 Characterization techniques

The crystal phase of the raw material and products was determined by powder X-ray diffraction (XRD, Bruker D8, Cu K_α radiation). The sample morphology was evaluated by transmission electron microscopy (TEM, Philips Tecnai G220 S-TWIN) at 200 kV. The textural properties were studied by N_2 adsorption-desorption measurements (ASAP 2020M) at liquid nitrogen temperature. Before analysis, the samples were degassed for 2 h at 150 °C under vacuum. The gold content of catalysts was detected by inductively coupled plasma optical emission spectrometer (ICP-OES, Optima 2000DV, USA).

1.3 Catalytic performance

Catalytic activity measurements were performed for the reduction of PNP to *p*-aminophenol (PAP) by $NaBH_4$ (liquid phase) at room temperature. The typical reduction procedure was carried out as follows: 50 mg Au/TiO_2 catalyst was quickly added into 60 ml aqueous solution mixed PNP (3 mmol/L) and $NaBH_4$ (0.05 mol/L), and then the mixture was vigorously stirred at room temperature until the yellow solution became colorless. The reduction process was monitored by measuring the extinction of solution at 400 nm as a function of time using a spectrophotometer (UNICO UV-2802S).

2 Results and discussion

2.1 Structure properties of catalysts

The phase constitutions of TiO_2 and the gold loaded samples were shown in Fig. 1. Obviously, we can find that almost all the diffraction peaks of the Au/TiO_2 samples can be indexed to (101), (004), and (200) peaks, corresponding to anatase type TiO_2 (JCPDS 21-1272). (110) and (101) peaks of rutile type TiO_2 were also detected in Au/P25 and Au/P25-R, indicating the mixed phase nature of commercial P25 titania. Besides anatase phase, characteristic peaks of TiO_2(B) phase were also confirmed in Fig. 1(1) and (2), which was consistent with our previous work [14–16]. Moreover, no rutile type TiO_2 were observed in Au/mb-TiO_2 after thermal treatment, which reflected the high phase stability of mb-TiO_2. No gold peaks were shown in the XRD patterns, which might be attributed to the high dispersion of gold and/or the very low gold loading.

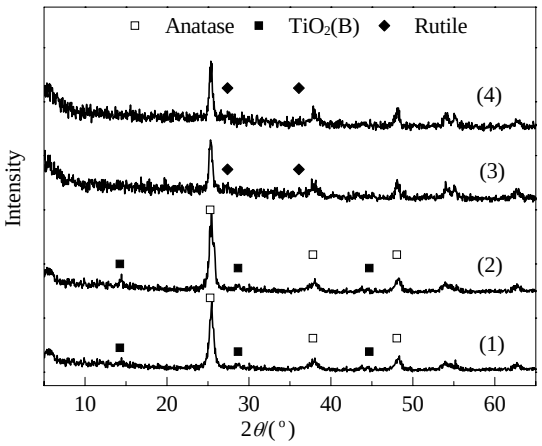

Fig. 1. XRD patterns of gold catalysts supported on mb-TiO_2 (1, 2) and P25 (3, 4) before (1, 3) and after (2, 4) high temperature treatments.

N_2 adsorption-desorption isotherms of mb-TiO_2, Au/mb-TiO_2, and Au/mb-TiO_2-R samples were shown in Fig. 2. These three samples have similar type IV isotherms. The N_2 adsorption amounts are nearly unchanged after loading gold and treating at high temperature, indicating that the mesoporous architecture was well maintained not only after gold loading but even after thermal treatment at 500 °C for 2 h. It's a crucial and positive factor for developing thermal stable gold catalyst. Meanwhile, the loaded gold nanoparticles were considered to be in a well dispersed

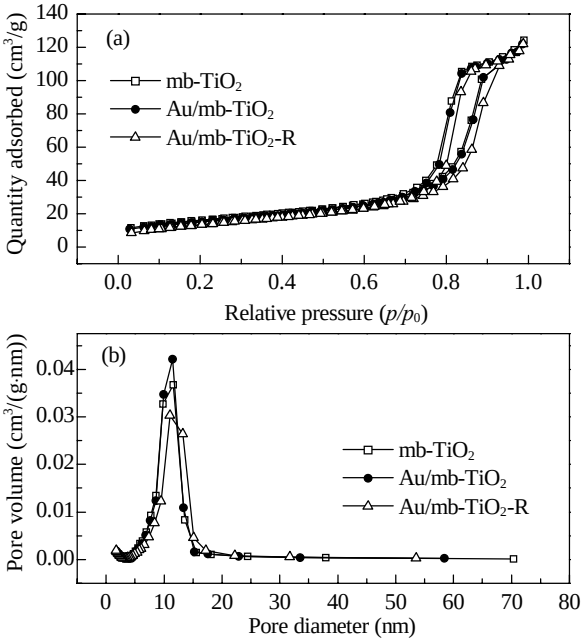

Fig. 2. N_2 adsorption-desorption isotherms (a) and pore size distributions (b) of mb-TiO_2, Au/mb-TiO_2, and Au/mb-TiO_2-R.

condition since the BET surface area and pore volume of the catalyst were almost the same as the titania support itself (shown in Table 1). The nanopores of the titania support was not easily blocked by the gold nanoparticles. That might be attributed to the rather larger pore size compared with the gold particle size and also the low gold loading amount in the catalyst. These results were first proved by the pore size distributions of these samples calculated by applying the BJH approach to the desorption branches of the corresponding isotherms, as shown in Fig. 2. The pore size distributions of all the samples were relatively narrow and centered at around 10 nm. There is only a small change in the pore size distribution for the sample after high temperature treatment, which was attributed to the slight growth of the titania nanocrystals. Table 1 summarized the physical properties of the supports and catalysts. Specifically, the BET surface area of mb-TiO_2 was 56.1 m^2/g, and slightly higher than that of commercial P25 (50.2 m^2/g). Moreover, the BET surface areas for both samples were not decreased obviously after loading gold and the further high temperature treatment.

Table 1 Chemical component, physical properties, average gold particle size, and rate constant of the samples

Sample	BET surface area (m^2/g)	BJH pore diameter (nm)	Pore volume (cm^3/g)	Actual loading of gold (%)	Average gold particle size (nm)	Rate constant of PNP reduction (min^{-1})
mb-TiO_2	56.1	11.6	0.193	—	—	—
Au/mb-TiO_2	53.5	11.5	0.189	1.960	6.6	0.151
Au/mb-TiO_2-R	49.6	11.0	0.189	1.960	7.3	0.152
P25	50.2	—	—	—	—	—
Au/P25	48.3	—	—	1.965	6.4	0.134
Au/P25-R	44.4	—	—	1.970	11.0	0.097

Electron microscopy techniques were used to investigate the microstructures and morphologies of both the titania support and the gold nanoparticles. TEM image of a typical mb-TiO_2 sample is shown in Fig. 3(a). The nanofibrous morphology was derived from the titanate precursor. Most of the samples were nanofibers with uniform size and had good nanofiber morphology, their average diameter was 0.1–0.3 μm and the average length was 1.5–5.0 μm. A deep insight into the fine structure of Au/mb-TiO_2 and Au/mb-TiO_2-R can be obtained by further TEM and HRTEM observations. Figures 3(b) and (d) showed the larger scale TEM images of Au/mb-TiO_2 and Au/mb-TiO_2-R, respectively. It reveals that gold loaded nanofibers kept the same morphology as mb-TiO_2 and the gold nanoparticles were well dispersed both on the outer surface and in the mesopores of mesoporous titania nanofibers, even after high temperature treatment. In addition, we focused on the particle size distributions of the gold nanoparticles before and after thermal treatment. On our previous assumption (from N_2 adsorption-desorption results), the particle size of gold might be less than the pore diameter of the titania support, thus, numerous 5–15 nm diameter bright spots in Figs. 3(b) and (d) must correspond to the mesopores of mb-TiO_2, which were well arranged along the longitudinal direction of the nanofiber. In the same direction, 20–30 nm wide nanocrystallites aligned loosely, with mesopores presented between them. The dark spots in Figs. 3(b) and (d) were then considered as gold nanoparticles. That was also proved by a typical HRTEM investigation of a single gold nanoparticle on the Au/mb-TiO_2 sample, shown in Fig. 3(c). The *d* spacing of the ellipsoidal particle was measured as 0.23 nm, which was considered as the typical (111) plane distance of metallic gold. Furthermore, at least three different directional lattice fringes of 0.23 nm were observed, which indicate that the gold nanoparticle is a highly crystallized polycrystalline cluster. In order to investigate the effect of high temperature treatment on the average gold particle size, more TEM images of Au/mb-TiO_2 and Au/mb-TiO_2-R were recorded. Though the similar preparation method was used as in the literatures [19,20], much larger gold particles were obtained in the present work. That might be attributed to the different preparation conditions. From our previous work [9], the gold loading is set as 1.0 wt%, which was insufficient for the precise average particle size calculation. However, the average gold particle size data which will be obtained in the present work should be much more reasonable because of the rather higher gold loading and the more uniform dispersion behavior. The average gold particle size was then calculated based on a total particle number of over 160 (shown in Table 1). It was found that after high temperature treatment, the gold nanoparticles size on mb-TiO_2 sample increased slightly from (6.6±1.6) nm to (7.3±1.4) nm, while that on commercial P25 titania nanopowder grew dramatically from (6.4±1.3) nm (Fig. 3(e)) to (11.0±2.1) nm (Fig. 3(f)). The histograms of gold particles size distribution for the catalysts were also shown in Fig. 4.

From the above TEM analysis, we can find that gold nanoparticles were more stable on the mesoporous titania nanofiber than on commercial P25 when the gold catalysts were treated at 500 °C for 2 h in helium atmosphere. This result was briefly attributed to the distinct support effect since the same synthesis parameters were introduced for

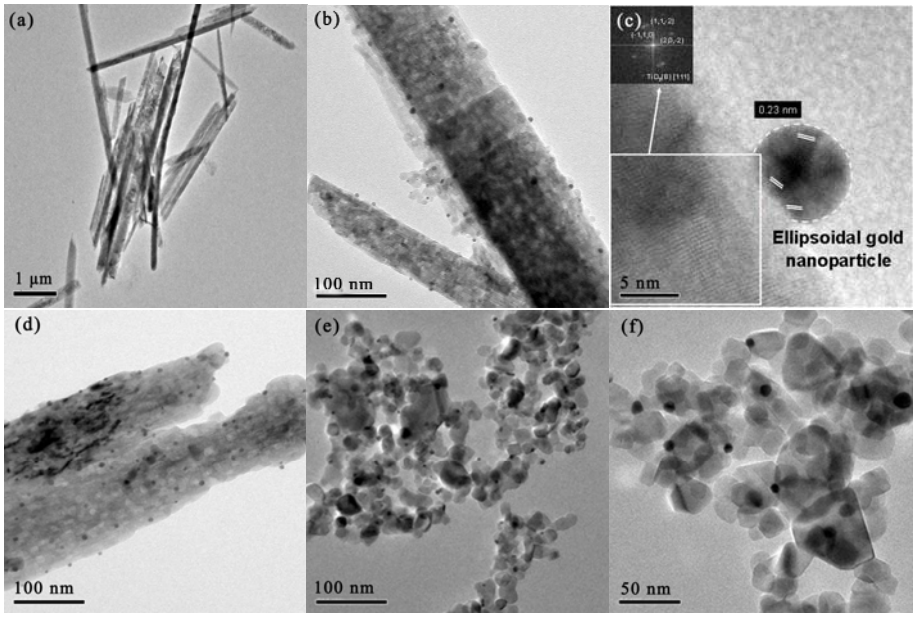

Fig. 3. TEM and HRTEM image of mb-TiO_2 (a), Au/mb-TiO_2 (b, c), Au/mb-TiO_2-R (d), Au/P25 (e), and Au/P25-R (f). Inset of (c) was the FFT image of the selected square area.

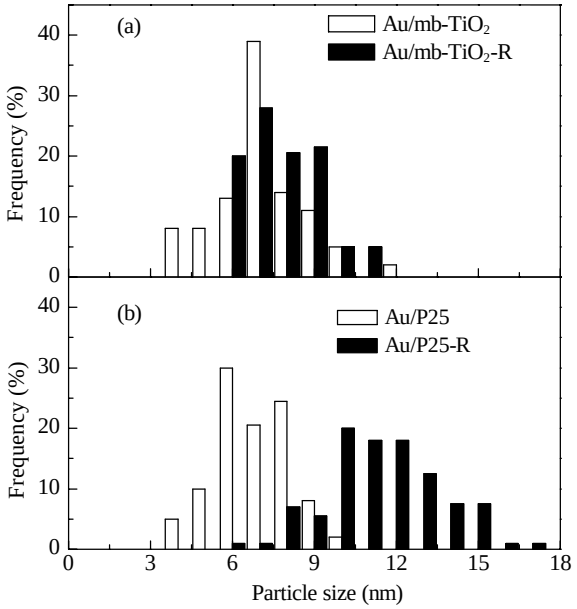

Fig. 4. Particle size distributions of Au/mb-TiO_2 and Au/P25. The total number of gold particles for calculation was 160.

both gold catalysts. Despite the gold catalysts supported on different types of supports [21,22], even for the ideal titania surface [23], the localized conditions (reduced, oxidized, or hydrated surfaces) will have great effect on the nucleation and bonding behaviors of nanogold clusters. In this work, the gold-titania interface of Au/mb-TiO_2 was different from any conventional Au/TiO_2 catalysts due to the peculiar TiO_2(B) coated anatase architecture of the mesoporous titania nanofiber. Recently, TiO_2(B) materials have received much attention for their outstanding performances in Li^+ ion battery [24], photocatalysis [15–17], and other environmental and energy related applications. However, to the best of our knowledge, TiO_2(B) materials have never been applied as a support of nanogold catalysts. Due to the metastable structural features and the lower thermodynamic stability of TiO_2(B) with respect to rutile, anatase, and brookite TiO_2, different metal support interaction was expected for Au/mb-TiO_2. The highly crystallized surface TiO_2(B) layers must play an important role in stabilizing the gold nanoparticles. Besides, the special mesoporous structure should also be taken into account. Considering that the pore diameter of mesoporous titania nanofiber was only slightly larger than the average particle size of gold, each gold nanoparticle should be located into one nanopore, which was constructed by the directionally three-dimensional assembly of titania nanocrystallites. The nanoarchitecture not only provided anchoring sites for the gold nanoparticles but also prolonged the distance between the nearest gold nanoparticles, which were all beneficial for preventing gold nanoparticles or atoms from migration and agglomeration.

2.2 PNP reduction

In order to understand the thermal stability of gold nanoparticles, PNP reduction was introduced as a model reaction to test the catalytic performances of the gold catalysts before and after thermal treatment. The catalytic activities of both the fresh and recalcined catalysts were presented in Fig. 5. The ratio of C_t and C_0, where C_t and C_0 represent PNP concentrations at time t and 0, respectively, was measured from the relative intensity of the respective absorbances. The linear relations of $\ln(C_0/C_t)$ versus time were observed for all the tested catalysts, indicating that the PNP reduction reaction followed first-order kinetics. The rate constants were also estimated from first order reaction kinetics using the slopes of straight lines in Fig. 5. The rate constants decreased from 0.134 to 0.097 min^{-1} when Au/P25 was recalcined at 500 °C, while the reaction rate on Au/mb-TiO_2 was nearly maintained as 0.15 min^{-1} (Table 1).

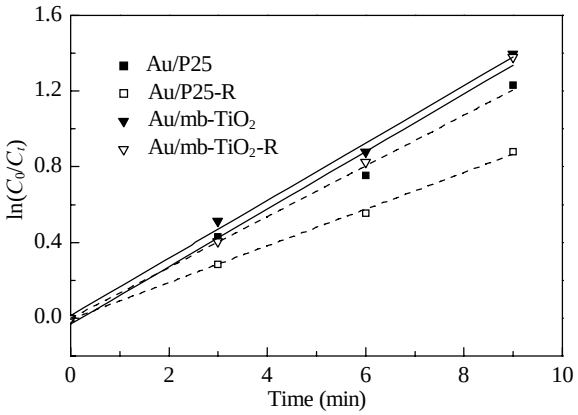

Fig. 5. Aqueous phase reduction of PNP by $NaBH_4$ over different gold catalysts.

The kinetic reaction rate constants, k, with different gold contents supported on mb-TiO_2 were shown in Fig. 6. In the range of 0.5%–2% loading amount, all the catalysts showed the similar activation after recalcination. This indicates that

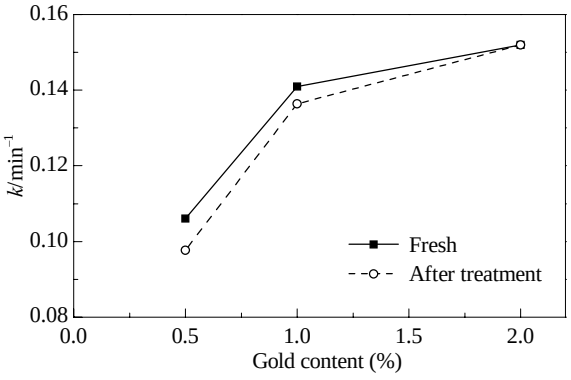

Fig. 6. The kinetic constant k of PNP reduction with different gold content supported on mb-TiO_2.

gold nanoparticles were more stable on the mesoporous titania nanofiber, which was consistent with the TEM results. It was reported that an increase of the particle size always leads to a decrease in the fraction of low coordination metal sites such as vertices, edges, and kinks, which can promote the adsorption of reactants and facilitate the reaction. The decrease of the reaction rate of Au/P25 might be attributed to this reason.

In this reaction, the gold nanoparticles played a key role as an electron transfer mediator between BH_4^- and PNP molecules [25]. The catalytic rate of the gold catalysts depends mainly on the availability of the active surface area. Here, for the gold nanoparticles supported on mesoporous titania nanofiber, the slight particle growth assured a similar total metal surface area available for the reactant adsorption and activation. This assumption was experimentally confirmed by the apparent size-controlled activity for the gold catalysts in PNP reduction. The stable PNP reduction performance and sinter-resistant behavior of Au/mb-TiO_2-R suggested that the titania nanofiber with the peculiar crystallographic structure and mesoporous nanoarchitecture could be used as an excellent sinter-resistant support material for other noble metal nanocatalysts.

3 Conclusions

The thermal stability of gold catalysts supported on the mesoporous titania nanofiber and commercial P25 materials were compared by using PNP reduction as a model reaction. From TEM images, it seems that gold nanoparticles size on the mesoporous titania nanofiber was nearly maintained after calcination at high temperature, while that supported on P25 changed dramatically. It indicates that titania nanofiber with the peculiar crystallographic structure and mesoporous nanoarchitecture could be used as an excellent sinter-resistant support material for other noble metal nanocatalysts. This result was also experimentally confirmed by the *p*-nitrophenol reduction reaction.

References

1 Haruta M, Kobayashi T, Sano H, Yamada N. *Chem Lett*, 1987, **2**: 405
2 Sinha A K, Seelan S, Tsubota S, Haruta M. *Angew Chem, Int Ed*, 2004, **43**: 1546
3 Prati L, Rossi M. *J Catal*, 1998, **176**: 552
4 叶青, 霍飞飞, 闫立娜, 王娟, 程水源, 康天放. 物理化学学报 (Ye Q, Huo F F, Yan L N, Wang J, Cheng Sh Y, Kang T F. *Acta Phys-Chim Sin*), 2011, **27**: 2872
5 Perez-Cabero M, El Haskouri J, Solsona B, Vazquez I, Dejoz A, Garcia T, Alvarez-Rodriguez J, Beltran A, Beltran D, Amoros P. *J Mater Chem*, 2010, **20**: 6780
6 Brown M A, Carrasco E, Sterrer M, Freund H J. *J Am Chem Soc*, 2010, **132**: 4064
7 Wang D H, Ma Z, Dai S, Liu J, Nie Z M, Engelhard M H, Huo Q S, Wang C M, Kou R. *J Phys Chem C*, 2008, **112**: 13499
8 张燕杰, 詹瑛瑛, 曹彦宁, 陈崇启, 林性贻, 郑起. 催化学报 (Zhang Y J, Zhan Y Y, Cao Y N, Chen Ch Q, Lin X Y, Zheng Q. *Chin J Catal*), 2012, **33**: 230
9 Zhu Y H, Li W, Zhou Y X, Lu X H, Feng X, Yang Z H. *Catal Lett*, 2009, **127**: 406
10 Ma Z, Brown S, Howe J Y, Overbury S H, Dai S. *J Phys Chem C*, 2008, **112**: 9448
11 Ma Z, Overbury S H, Dai S. *J Mol Catal A*, 2007, **273**: 186
12 苏继新, 张慎平, 马丽媛, 屈文, 张明博. 催化学报 (Su J X, Zhang Sh P, Ma L Y, Qu W, Zhang M B. *Chin J Catal*), 2010, **31**: 839
13 Tauster S J, Fung S C, Garten R L. *J Am Chem Soc*, 1978, **100**: 170
14 He M, Lu X H, Feng X, Yu L, Yang Z H. *Chem Commun*, 2004: 2202
15 Li W, Liu C, Zhou Y X, Bai Y, Feng X, Yang Z H, Lu L H, Lu X H, Chan K Y. *J Phys Chem C*, 2008, **112**: 20539
16 Li W, Bai Y, Liu C, Yang Z H, Feng X, Lu X H, van der Laak N K, Chan K Y. *Environ Sci Technol*, 2009, **43**: 5423
17 Bai Y, Li W, Liu C, Yang Z H, Feng X, Lu X H, Chan K Y. *J Mater Chem*, 2009, **19**: 7055
18 朱银华, 陈闪山, 陆小华, 杨祝红, 冯新, 汪怀远. 催化学报 (Zhu Y H, Chen Sh Sh, Lu X H, Yang Zh H, Feng X, Wang H Y. *Chin J Catal*), 2009, **30**: 421
19 Zanella R, Giorgio S, Henry C R, Louis C. *J Phys Chem B*, 2002, **106**: 7634
20 Zanella R, Giorgio S, Shin C H, Henry C R, Louis C. *J Catal*, 2004, **222**: 357
21 Comotti M, Li W C, Spliethoff B, Schuth F. *J Am Chem Soc*, 2006, **128**: 917
22 Dobrosz-Gomez I, Kocemba I, Rynkowski J M. *Appl Catal B*, 2008, **83**: 240
23 Matthey D, Wang J G, Wendt S, Matthiesen J, Schaub R, Laegsgaard E, Hammer B, Besenbacher F. *Science*, 2007, **315**: 1692
24 Armstrong A R, Armstrong G, Canales J, Bruce P G. *Angew Chem, Int Ed*, 2004, **43**: 2286
25 Lee J, Park J C, Song H. *Adv Mater*, 2008, **20**: 1523